Basic analysis of optimal images for the development of 4D radiotherapy system

Kazunori Miyaura[*1], Kouzou Murakami[2], Hiroyuki Watanabe[1], Yoshinori Ito[2] and Yoshikazu Kagami[2]

Abstract

Understanding respiratory motion is necessary for accurate dose administration during stereotactic body radiation therapy. Although four-dimensional (4D) computed tomography (4DCT) is useful for understanding respiratory movements, 4D radiotherapy with a time axis is required. However, reports on the evaluation of 4DCT remain lacking. Therefore, this study was designed to evaluate the basic physical characteristics of a respiratory-gated 4DCT helical scanning system (4D-HS) using MATLAB®. In this study, the physical characteristics were evaluated by examining the body-axis direction resolution, slice sensitivity profile (SSP), and volume change due to respiratory phase change and comparing multiplanar reconstruction profiles (MPRs) of slit phantoms. These characteristics were compared using normal helical scanning (N-HS). A 31% overestimation was observed in the volume fluctuation of 4D-HS based on the volume of N-HS. Furthermore, SSP with full width at half maximum (FWHM) and modulation transfer function (MTF) showed a similar resolution between 4D-HS and N-HS. The difference in FWHM is considered an offset by the voxel effect. In the MPR comparison, both 4D-HS and N-HS were visually identifiable up to a 0.5-mm slit. 4D-HS is a reconstruction system with excellent temporal resolution. Furthermore, its resolution follows respiratory dynamics and can continuously collect respiratory dynamics components. Our findings suggest the usefulness of 4D-HS in clinical practice.

Key words : 4DCT, helical scanning, respiratory motion, respiratory cycle

Introduction

High-precision three-dimensional (3D) original irradiation (i.e., 3D conformal radiotherapy (3D-CRT)) can be applied in radiation therapy because of its high accuracy in demonstrating respiratory motion; using 3D-CRT allowed the performance of stereotactic body radiation therapy (SBRT). During SBRT, the dose concentration is increased, which can improve local control and reduce doses to peripheral organs and thus adverse events. This treatment aims to irradiate large doses over a shorter time than conventional radiotherapy using fixed multi-gate irradiation or multi-orbit rotational motion irradiation[1]. Perform these methods within a 5-mm gap (fixed accuracy) of the irradiation center position for each irradiation time is necessary. Additionally, synchronizing or monitoring physiological respiratory exercises and internal movement of organs for irradiation and performing accuracy control against the difference during treatment are essential.

For this reason, an accurate and appropriate irradiation field setting, in accordance with the International Commission on Radiation Units and Measurements (ICRU) report 62, is required based on respiratory motion measurements and computed tomography (CT) photography methods[2]. Irradiation volume for small tumors subjected to body executive position irradiation is defined as follows: the planning target volume is obtained by adding the internal target volume (ITV) and setup margin; the ITV is obtained by adding the clinical target volume and internal margin (IM). SBRT is a multidirectional

* Corresponding author

✉ Kazunori Miyaura
  kmiyaura@med.showa-u.ac.jp

[1] Showa University Graduate School of Health Sciences, 1-5-8 Hatanodai, Shinagawa-ku, Tokyo 142-8666, Japan.
[2] Department of Radiology, Division of Radiation oncology, Showa University School of Medicine.

and radiation-accurate targeting technique for small tumors with localized body executives aiming to improve local control and reduce adverse events to surrounding organs[3,4].

Therefore, an accurate irradiation volume setting is required. ITV is composed of the IM; however, a large respiratory motion requires the addition of movements, which will lead to increased radiation. When a high dose is administered during SBRT, reducing the dose to the peripheral organs is difficult and may be inappropriate. Determining a method for capturing respiratory motion and organizing an ITV is important. Understanding the range of tumor migration based on respiratory migration allows easier and more appropriate formulations of ITV settings.

Several methods for managing respiratory motion during radiotherapy have been proposed[5]. In the thoracic region where respiratory motion is present, CT imaging during free respiration results in distorted images due to motion artifacts[6]; these motion artifacts induce contouring errors, which reduce the accuracy of dose calculation[3,7]. Different methods for managing respiratory movements can be applied after respiratory motion is assessed using SBRT; however, the accuracy of each method requires verification at each facility[5]. To ensure respiratory motion, a planned CT may be useful to obtain IM; however, the accuracy depends on the CT imaging method. Studies have reported the effectiveness of using 4DCT and setting the ITV from the IM for respiratory motion in improving the diagnostic accuracy by analyzing the tumor position in each respiratory phase[8-10]. Moreover, studies have reported the quality control and accuracy assurance of CT equipment in radiotherapy[11,12]. However, of the 4DCT imaging methods, studies evaluating and verifying the accuracy of the physical properties of the 4DCT helical scanning system (4D-HS) remain lacking.

Therefore, we examined the basic physical properties of 4D-HS during the application in respiratory exercises of lung tumors in body executive position irradiation.

Methods and materials

In this study, we conducted three processes to evaluate the following physical properties of 4D-HS and verify its accuracy: 1) time and spatial resolution, 2) change in target volume calculated from reconstructed images in the respiratory phase, and 3) examination of spatial decomposition by multiplanar reconstruction (MPR). The reconstructed CT images

were analyzed using MATLAB_R2015a (MathWorks, Massachusetts, U.S.).

1-1. Time and spatial resolution

The slice sensitivity profile (SSP) of time and spatial resolution was measured in the body-axis direction of the 4D-HS, and the resolution of each SSP was examined. The SSP shows the resolution of the profile curve in the body-axis direction.

In this study, a CT device, AquilionLB (Canon Medical, Tokyo, Japan), and respiratory motion phantom (RM Phantom) (QUASAR, Ontario, Canada) were used to determine the time and spatial resolution. A micro-coin phantom (Kyoto Science Company, Kyoto, Japan) was installed in the body-axis drive of the RM Phantom, which was driven for 4D-HS; furthermore, 0.05-mm- and 1-mm-thick φ were installed. Next, the driving of the RM Phantom was discontinued, and normal helical scanning (N-HS) was performed. Each image reconstruction was performed to obtain an image of each 4D-HS phase and an image from N-HS. The parameters of the microphantom imaging protocol were a tube voltage of 120 kV, tube current of 50 mA, scan time of 0.5 s/rot, imaging slice thickness of 1 mm, scan field of view (FOV) of 550 mm, reconstruction slice thickness of 1.0 mm, and reconstruction slice spacing of 0.1 mm.

The respiratory phase of the RM Phantom was 0% at the starting point, which reached 50% at the maximum intake of respiratory signal in the respiratory phase. The 4D-HS was reconstructed using a 50% respiratory phase. The RM Phantom collected data from two separate situations. Situation 1 was during resting breath in which the respiratory cycle was 12 cycles/min (cpm) with a RM of 2 cm. Contrarily, situation 2 was during a short cycle in which the respiratory cycle was 20 cpm with a RM of 2 cm.

1-2. Change in the target volume calculated from the reconstructed images using the respiratory phase

In 4D-HS photography, steep tumor movement creates motion artifacts, which cause shape deformations in the image, indicating fluctuations in the tumor volume. Then, a 3D object with a known volume was captured. The effect of movement size on tumor volume fluctuation was examined.

An imaging insert phantom (QUASAR), a 30-mm cube, a 20-mm diameter (large sphere), and a 10-mm (small sphere) sphere were attached to the body-axis drive portion of the RM Phantom to drive the RM Phantom for 4D-HS. Next, the drive of the RM Phantom was discontinued, and N-HS was performed.

The respiratory phase of the RM Phantom was 0% at the starting point and reached 50% during the maximum intake of the respiratory signal acquired by the respiratory management system.

The 4D-HS was reconstructed every 10% of the respiratory phase from 0% to 50%.

1-3. Examination of spatial decomposition using MPR

In 4D-HS photography, steep tumor movement can cause motion artifacts, which cause shape deformations in the image. Therefore, a slit phantom image was captured, MPR was created, and the spatial resolution of 4D-HS and N-HS was examined.
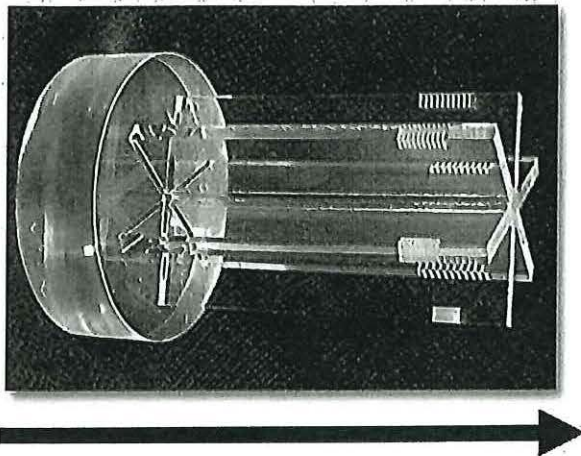
CT scan direction

Fig. 1. Slit phantom appearance
0.7-, 0.6-, 0.5-, 0.4-, 0.3-, and 0.2-mm slits are engraved on the plate-shaped acrylic.

MPR is an image-processing method that uses a computer to process cross-sectional image data obtained by irradiating X-rays from one direction and reconstructs the cross-sectional image when viewed from various directions. A 3D image can be created by repeating the same process.

A self-made slit phantom (slit widths of 0.7, 0.6, 0.5, 0.4, 0.3, and 0.2 mm) was attached to the body-axis drive part of the RM Phantom, which was driven and photographed using 4D-HS. Next, the drive of the RM Phantom was discontinued, and an N-HS image was captured.

The respiratory phase of the RM Phantom was 0% at the starting point of the maximum intake of the respiratory signal acquired by the respiratory management system; the respiratory phase was 50% at the maximum air intake.

The 4D-HS image was reconstructed using a respiratory phase of 50%. The appearance of the slit phantom used is shown in Figure 1.

Results

2-1. Time and spatial resolution

SSP measurements and full width at half maximum (FWHM) examinations were performed to compare the body-axis resolution between 4D-HS and N-HS. FWHM is the difference between the two values of the independent variables at which the dependent variable is equal to half its maximum value. The slice thickness of the image reconstruction was 0.5 mm. The SSP of the
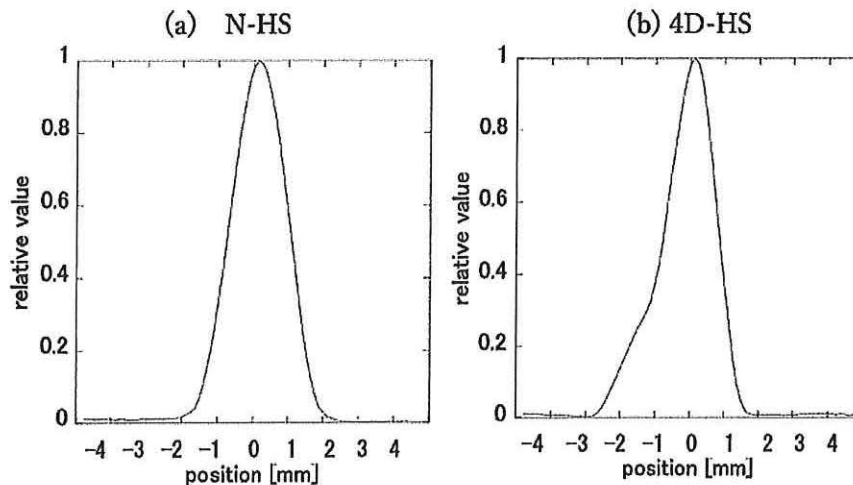

Fig. 2. Results of slice sensitivity profile (SSP) with QUASAR respiratory synchronous phantom (RM Phantom) under situation 1. The x-axis represents the body-axis direction, and the y-axis represents the computed tomography (CT) value of the coin phantom as a relative value.
a : Result for normal helical scanning (N-HS).
b : Result for respiratory-gated helical scan four-dimensional system (4D-HS).

RM Phantom under situation 1 is shown in Figure 2. The FWHM of the SSP in 4D-HS and N-HS was 1.50 mm and 1.48 mm, respectively. The shape was observed to be in good agreement. The SSP under situation 2 is shown in Figure 3. The shape of the waveform was lost. A larger shape collapse was observed in phase 0% than in phase 50%; furthermore, difficulties were encountered in identifying peaks and calculating and evaluating FWHM.

2-2. Change in the target volume calculated from the reconstructed images using the respiratory phase

Volume variations were measured for the reconstructed images of 4D-HS and N-HS. The slice thickness of the image reconstruction was 0.5 mm. The volume (V) was calculated using the following equation by adding the cross-sectional area s_i of the region of interest (ROI) surrounding the target volume in the ith slice and the distance d_i to the ith and $i+1^{th}$ slices:

$$V = \sum_{i=1}^{n} s_i d_i$$

where s_i indicates the ROI cross-sectional area set on slice i and d_i indicates the intervals up to slice $i+1$ slice.

In 4D-HS, the volume of each reconstructed image was calculated every 10% of the steps in the respiratory phase of 0%–50% as follows:

$$\Delta V_{dev}(\%) = \frac{(V_{4DHS\_resp} - V_{NHS})}{V_{NHS}} \times 100$$

Based on the volume of N-HS, V_{dev} was calculated as the change in the volume of the respiratory phase in each solid. The results of the volume changes are shown in Tables 1, 2, and 3; the graphical representation of the volume change is shown in

Figure 4. In the graph, the x-axis represents the respiratory phase of 4D-HS, and the y-axis represents the volume fluctuation based on the volume of N-HS. Furthermore, 0% and 50% of the respiratory phase correspond to the maximum inspiratory and expiratory positions, respectively. In the volume change due to the respiratory phase of a cube, the maximum V_{dev} was 12.2% and 1.7% at Resp_20% and Resp_50% minimum, respectively. In the volume change due to the respiratory phase of a large sphere, the maximum V_{dev} was 15.9% and 3.6% for Resp_20% and Resp_0%, respectively. Finally, the maximum V_{dev} for the volume change due to the respiratory phase of the small sphere was 31.7% and 4.5% for Resp_20% and Resp_0% minimum, respectively.

An increase in the volume change was observed as the respiratory phase progressed; particularly, V_{dev} maximized at Resp_20% to Resp_30%, followed by a decrease. Variations in the width of the volume change were observed, represented by a graph similar to a sine wave.

2-3. Examination of spatial resolution using MPR

The spatial resolution in the body-axis direction was compared using MPR in 4D-HS and N-HS.

Using image analysis, MPRs were created from the reconstructed images, which were searched for profiles. The results are shown in Figures 5–10.

Visual observations were identifiable with slits with 0.7-, 0.6-, and 0.5-mm slit widths. The profiles with 0.7-mm and 0.6-mm slit widths were observed to have the same slit shape and resolution for both 4D-HS and N-HS. The resolution of N-HS was observed up to the slit width of 0.5 mm. However, a difference in
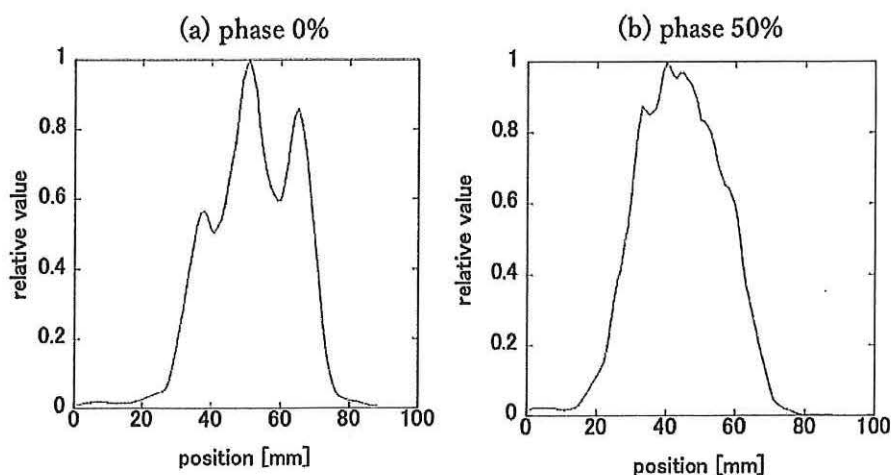

Fig. 3. Slice sensitivity profile (SSP) results with QUASAR respiratory synchronous phantom (RM Phantom) under situation 2. The x-axis represents the body-axis direction, and the y-axis represents the computed tomography (CT) value of the coin phantom as a relative value.
a : Result for phase 0%, b : Result for phase 50%.

Table 1. Volume changes due to differences in the respiratory phase in a cube

Scan type		V[mm³]	V_{dev}[%]
N-HS	–	29099.9	–
4D-HS	Resp_ 0%	29624.7	1.8
	Resp_10%	30910.2	6.2
	Resp_20%	32659.5	12.2
	Resp_30%	31008.9	6.6
	Resp_40%	29770.0	2.3
	Resp_50%	29587.8	1.7

N-HS, normal helical scanning; 4D-HS, respiratory-gated helical scan four-dimensional system.

Table. 2. Volume changes due to differences in the respiratory phase in a large sphere

Scan type		V[mm³]	V_{dev}[%]
N-HS	–	4594.3	–
4D-HS	Resp_ 0%	4758.1	3.6
	Resp_10%	5161.8	12.4
	Resp_20%	5324.4	15.9
	Resp_30%	5188.3	12.9
	Resp_40%	4815.8	4.8
	Resp_50%	4786.9	4.2

N-HS, normal helical scanning; 4D-HS, respiratory-gated helical scan 4D system.

Table 3. Volume change due to differences in the respiratory phase in a small sphere

Scan type		V[mm³]	V_{dev}[%]
N-HS	–	619.4	–
4D-HS	Resp_ 0%	647.1	4.5
	Resp_10%	765.9	23.7
	Resp_20%	815.5	31.7
	Resp_30%	790.1	27.6
	Resp_40%	665.6	7.5
	Resp_50%	669.0	8.0

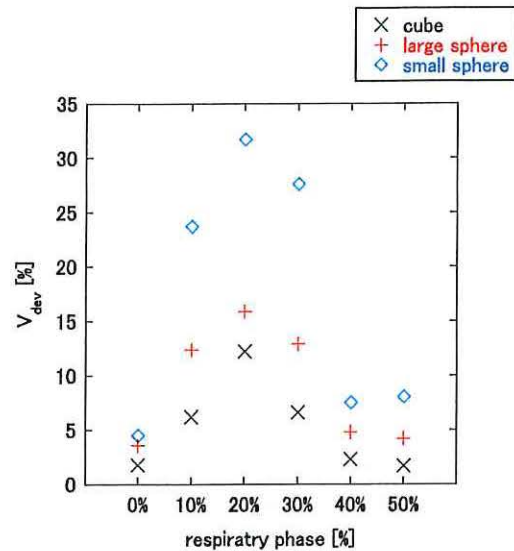N-HS, normal helical scanning; 4D-HS, respiratory-gated helical scan 4D system.

Fig. 4. Volume change of respiratory-gated helical scan four-dimensional system (4D-HS) relative to normal helical scanning (N-HS) using the respiratory phase. ✕ is the volume change of the cube, + is the large sphere, and ◇ is the small sphere. The x-axis represents the respiratory phase, and the y-axis represents each volume change.

Discussion

In 4DCT photography, a dynamic object is reconstructed as a static image. Normally, when an image of a moving object is captured, the edges are blurred, and the shape is changed, resulting in a decreased spatial resolution. Furthermore, the time resolution is reduced depending on the imaging time. When helical scanning is performed, measuring the spatial resolution of the body axis and SSP is recommended[13]. Furthermore, an SSP is created since the RM Phantom is driven in the body-axis direction, and an examination of the time and spatial resolution in the body axis is conducted.

The significance of SSP measurements includes verification of the set slice thickness, effects of focus size and the image reconstruction method, influence of the pitch factor (helical scan), and other information (e.g., SSP shape and contrast)[14, 15]. The calculated modulation transfer function (MTF) results are shown in Figure 11. MTF is a function of spatial frequency and provides information on how the resolution characteristics change at various spatial frequencies. Situation 1 of the RM Phantom showed that the FWHM of the SSP between 4D-HS and N-HS was within 1.3%; similar results were obtained when the partial volume effect was measured. However, a difference in the base spread was observed when the profile shape was compared. 4D-HS and N-HS had different imaging conditions, including

the profile shape was observed between 4D-HS near the center of the slit and the vicinity of the margin; particularly, a reduced resolution was observed near the margin. Visual evaluation and profiling of 4D-HS and N-HS were difficult when slit widths of 0.4, 0.3, and 0.2 mm were used.
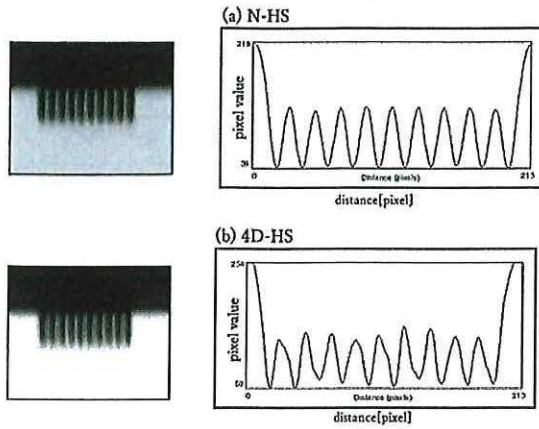
Fig. 5. Images and profiles with multiplanar reconstruction profile (MPR) with a slit width of 0.7 mm. The sagittal plane of MPR and its profile are shown.
a : Result for normal helical scanning (N-HS).
b : Result for respiratory-gated helical scan four-dimensional system (4D-HS).
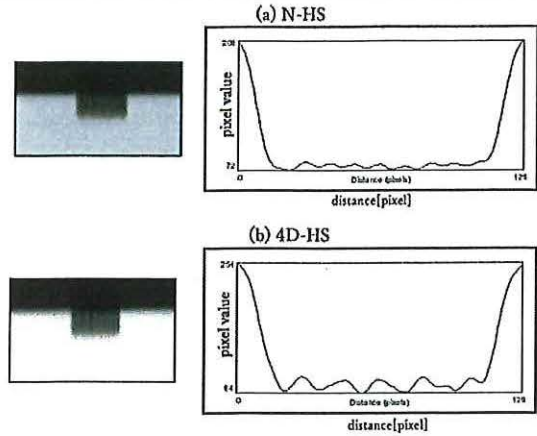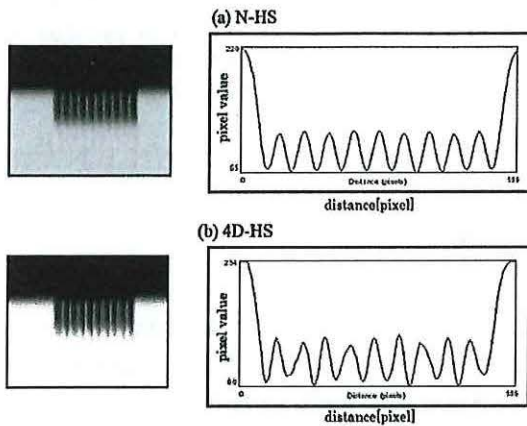

Fig. 8. Images and profiles with multiplanar reconstruction profile (MPR) with a slit width of 0.4 mm. The sagittal plane of MPR and its profile are shown.
a : Result for normal helical scanning (N-HS).
b : Result for respiratory-gated helical scan four-dimensional system (4D-HS).

Fig. 6. Images and profiles with multiplanar reconstruction profile (MPR) with a slit width of 0.6 mm. The sagittal plane of MPR and its profile are shown.
a : Result for normal helical scanning (N-HS).
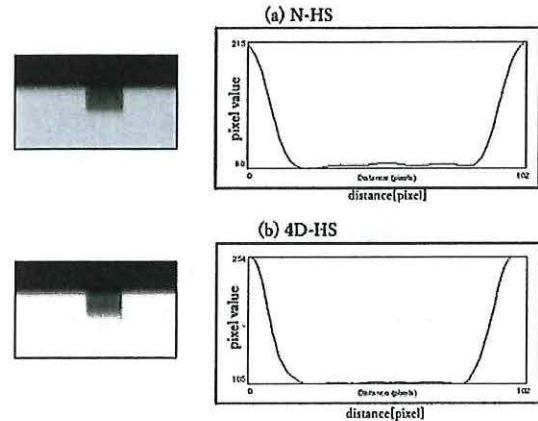b : Result for respiratory-gated helical scan four-dimensional system (4D-HS).

Fig. 9. Images and profiles with multiplanar reconstruction profile (MPR) with a slit width of 0.3 mm. The sagittal plane of MPR and its profile are shown.
a : Result for normal helical scanning (N-HS).
b : Result for respiratory-gated helical scan four-dimensional system (4D-HS).
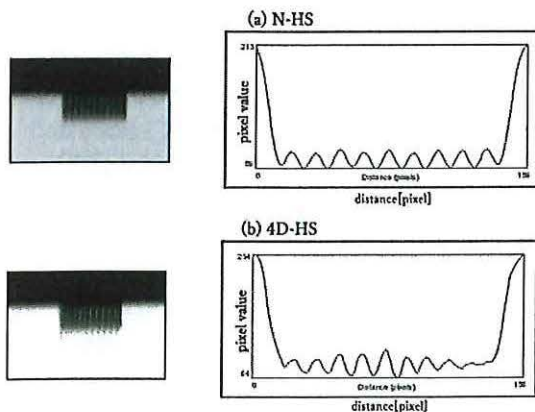

Fig. 7. Images and profiles with multiplanar reconstruction profile (MPR) with a slit width of 0.5 mm. The sagittal plane of MPR and its profile are shown.
a : Result for normal helical scanning (N-HS).
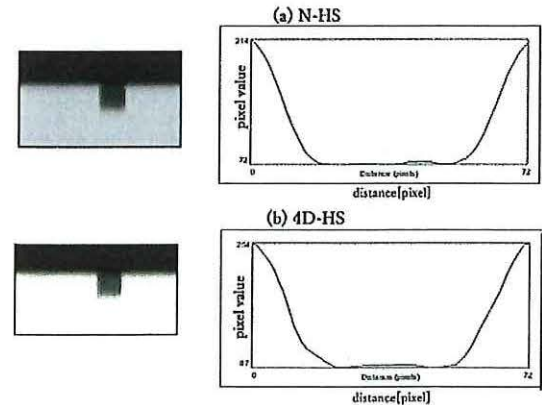b : Result for respiratory-gated helical scan four-dimensional system (4D-HS).

Fig. 10. Images and profiles with multiplanar reconstruction profile (MPR) with a slit width of 0.2 mm. The sagittal plane of MPR and its profile are shown.
a : Result for normal helical scanning (N-HS).
b : Result for respiratory-gated helical scan four-dimensional system (4D-HS).
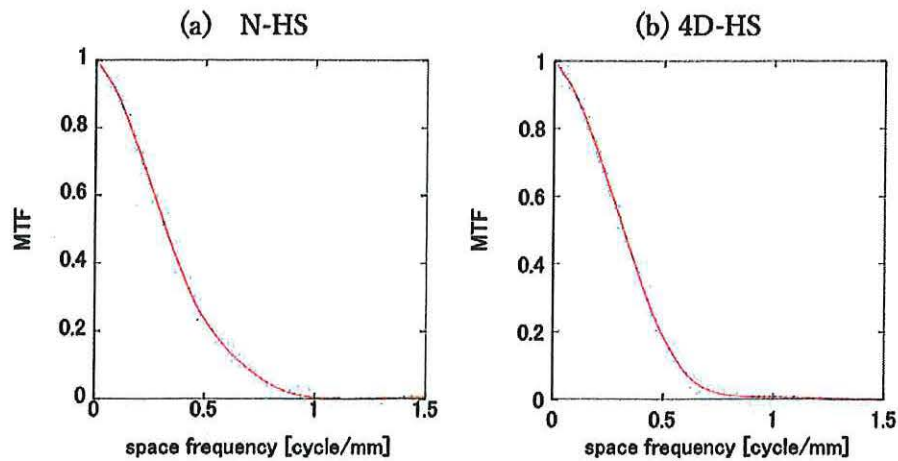
Fig. 11. Modulation transfer function (MTF) results with the RM Phantom under situation 1. The x-axis represents the space frequency, and the y-axis represents the MTF.
a : Result for normal helical scanning (N-HS).
b : Result of respiratory-gated helical scan four-dimensional system (4D-HS).

pitch factor; therefore, the FWHM alone may be an insufficient parameter to accurately compare resolutions. Considering this, MTF was added to compare the imaging modalities.

MTF has the advantage of confirming the response for each frequency and therefore can provide a detailed evaluation of the difference in resolution in body-axis direction, which is not easily understood when only comparing the shape and indicator value. Comparisons were made at 50% and 10% MTF. The 50% MTF between 4D-HS and N-HS matched within 1.5%. Contrarily, a difference was observed when comparing 10% MTF of the two imaging modalities. Particularly, N-HS has a slightly better spatial resolution in the body axis than 4D-HS; however, the results may be considered comparable when reproducibility, such as the installation accuracy in measurement, is considered. The spatial resolution of 4D-HS greatly depends on the respiratory cycle and RM amount; this was shown in situation 2 in which the spatial resolution was extremely reduced when the respiratory cycle (20 cpm) and period were short and the movement per unit time was large. Thus, almost similar results were obtained between 4D-HS and N-HS when evaluated using resolution frequencies of up to 0.5 cycle/mm, which was the limit resolution frequency in MTF.

The movement of an object causes blurring when CT images are captured causing shape changes, blurred edges, and volume changes[7, 16-18]. In radiation therapy, dose–volume histogram (DVH) parameters are used to evaluate the dose of targets and organs. Therefore, accurate contouring may not be achieved when the volume is blurred due to artifact movement, which may cause uncertainty in dose evaluation, resulting in under- or over-irradiation.

Regarding the change in the target volume calculated from the reconstructed image of the respiratory phase, a large variation was observed from Resp_20% to Resp_30%; however, Resp_0% and Resp_50% demonstrated almost equal results. The respiratory signal of the RM Phantom was a sine wave, with a drive demonstrating a linear motion toward the body axis. Therefore, Resp_20% and Resp_30% were areas where acceleration in the movement of the RM Phantom was observed. Furthermore, a rapid increase in the V_{dev}, shape changes and volume fluctuations were observed due to the inability to cope with this movement. Moreover, the width of the volume variation was shown to be significant when the volume is small. An inverse relationship was observed between the size of the target volume and the variation in volume variation (Fig. 12). Furthermore, a decrease in the time resolution was observed when the imaging time increased in response to the movement speed of the object. That is, it becomes an image that adds the components of movement, with the possibility of being drawn large; likewise, the volume may be large with blur and shape changes. In a sphere with a small volume, noise increases due to movement, emphasizing the shape change of the edge portion blur with an increase in volume.

Considering the following points is necessary when constructing an MPR for examining the spatial resolution: the use of minimum slice thicknesses and changes in beam configuration; helical pitch, which may affect resolution; and spatial resolution, which may change depending on the FOV and voxel size[19].
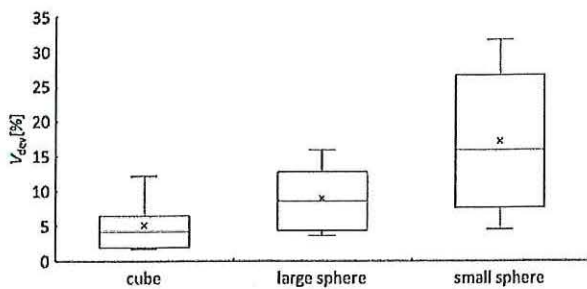
Fig. 12. Evaluation of volume change in respiratory-gated helical scan four-dimensional system (4D-HS) relative to that in normal helical scanning (N-HS) using the respiratory phase

The difference in volume change for each respiratory phase is represented by a box plot for each solid. The x-axis represents each structure, and the y-axis represents the rate of volume change. ✕ represents the median.

In this study, we evaluated 4D-HS and N-HS based on the assumption that they were not measured to meet the aforementioned conditions.

In this study, the time and spatial resolution in the body-axis direction in N-HS and 4D-HS, change in the target volume calculated from the reconstructed images using the respiratory phase, and spatial resolution using MPR were examined. At 12 cpm, a human's resting breathing cycle, N-HS and 4D-HS had the same resolution. However, the spatial resolution of 4D-HS decreased compared with that of N-HS in the respiratory phase when the respiratory cycle was significantly shortened or when the acceleration of movement was large.

Particularly, the time and spatial resolutions of 4D-HS were equivalent to those of N-HS when evaluated within the respiratory cycle range under the limit based on the remaining breathing cycle.

Conflict of interest disclosure

The authors have no conflicts of interest regarding this study.

References

1. Benedict SH, Yenice KM, Followill D, *et al*. Stereotactic body radiation therapy: the report of AAPM Task Group 101. *Med Phys*. 2010;**37**:4078-4101.
2. International Commission on Radiation Units and Measurements. Prescribing, recording, and reporting photon beam therapy. ICRU report 62. Bethesda Md: International Commission on Radiation Units and Measurements; 1999.
3. Davis AT, Palmer AL, Pani S, *et al*. Assessment of the variation in CT scanner performance (image quality and Hounsfield units) with scan parameters, for image optimisation in radiotherapy treatment planning. *Phys Med*. 2018;**45**:59-64.
4. Ford JM, Decker SJ. Computed tomography slice thickness and its effects on three-dimensional reconstruction of anatomical structures. *J Forensic Radiol Imaging*. 2016;**4**:43-46.
5. American Association of Physicists in Medicine. The management of respiratory motion in radiation oncology. Report of AAPM task group 76. 2006.
6. Keall PJ, Kini VR, Vedam SS, *et al*. Potential radiotherapy improvements with respiratory gating. *Australas Phys Eng Sci Med*. 2002;**25**:1-6.
7. Chen GT, Kung JH, Beaudette KP. Artifacts in computed tomography scanning of moving objects. *Semin Radiat Oncol*. 2004;**14**:19-26.
8. IAEA. Quality assurance programme for computed tomography: diagnostic and therapy applications. Vienna: International Atomic Energy Agency; 2012.
9. Ford EC, Mageras GS, Yorke E, *et al*. Respiration-correlated spiral CT: a method of measuring respiratory-induced anatomic motion for radiation treatment planning. *Med Phys*. 2003;**30**:88-97.
10. Vedam SS, Keall PJ, Kini VR, *et al*. Acquiring a four-dimensional computed tomography dataset using an external respiratory signal. *Phys Med Biol*. 2003;**48**:45-62.
11. Kalender WA. X-ray computed tomography. *Phys Med Biol*. 2006;**51**:R29-R43.
12. American Association of Physicists in Medicine. Report no.1 Phantoms for performance evaluation and quality assurance of CT scanners. Chicago: American Association of Physicists in Medicine; 1977.
13. Makmur IWA, Setiabudi W, Anam C. Evaluation Ketebalan irisan (slice thickness) pada pesawat CT-scan single slice. *J sains dan matematika*. 2013;**21**:42-47.
14. Monnin P, Sfameni N, Gianoli A, *et al*. Optimal slice thickness for object detection with longitudinal partial volume effects in computed tomography. *J Appl Clin Med Phys*. 2017;**18**:251-259.
15. Somigliana A, Zonca G, Loi G, *et al*. How thick should CT/MR slices be to plan conformal radiotherapy? A study on the accuracy of three-dimensional volume reconstruction. *Tumori*. 1996;**82**:470-472.
16. Nakamura M, Narita Y, Sawada A, *et al*. Impact of motion velocity on four-dimensional target volumes: a phantom study. *Med Phys*. 2009;**36**:1610-1617.
17. Balter JM, Haken RKT, Lawrence TS, *et al*. Uncertainties in CT-based radiation therapy treatment planning associated with patient breathing. *Int J Radiat Oncol Biol Phys*. 1996;**36**:167-174.
18. Shimizu S, Shirato H, Kagei K, *et al*. Impact of respiratory movement on the computed tomographic images of small lung tumors in three-dimensional (3D) radiotherapy. *Int J Radiat Oncol Biol Phys*. 2000;**46**:1127-1133.
19. Gulliksrud K, Stokke C, Martinsen ACT. How to measure CT image quality: Variations in CT-numbers, uniformity and low contrast resolution for a CT quality assurance phantom. *Phys Med*. 2014;**30**:521-526.